A hybrid particle and coupled moment-of-fluid level set method for multiphase flows

Cody Estebe

April 2, 2024

Particle Level Set Moment of Fluid

- A new algorithm that hybridizes massless marker particles with the coupled level set moment-of-fluid method to improve the interface reconstruction in multiphase flow problems is proposed
- Volume-preserving
- Applicable to N-phase flow involving ≥ 2 materials
- Benchmark tests including rigid body motion, two phase flow, and multiphase flow problems undergoing phase change and 'triple-points'

Background

Moment-of-Fluid method (MOF) [3, 9, 6]

- advect volume fractions and centroids to reconstruct interface
- local reconstruction procedure
- susceptible to checkerboard instability

Continuous Moment-of-Fluid method (CMOF)[17]

- non-local 'supercell' reconstruction to combat checkerboard instability

Particle Level Set method (PLS) [4]

- improve mass conservation by hybrid 'interface-capturing'/'interface-tracking'
- uses independently advected Lagrangian marker particles to correct level set

Particle Level Set Moment-of-Fluid method (PLSMOF)

- instead of CMOF supercell, use Lagrangian marker particles seeded both on and near interface
- particles used to reconstruct interface

[3] (Dyadechko, Shashkov 2005), [9] (Li et al. 2015), [6](Jemison et al. 2013),
[17] (Ye et al. 2023),
[4] (Enright et al. 2002)

Governing Equations 1

We define the rigid and fluid materials using the following multimaterial level set formulation:

$$\phi_{m_{\text{rigid}}}(\boldsymbol{x}, t) = \begin{cases} > 0 & \boldsymbol{x} \in \text{material } m_{\text{rigid}}, \\ \leq 0 & \text{otherwise}, \end{cases}$$

$$\phi_{m_{\text{fluid}}}(\boldsymbol{x}, t) = \begin{cases} > 0 & \boldsymbol{x} \in \text{material } m_{\text{fluid}} \cup m_{\text{fluid,ghost}}, \\ \leq 0 & \text{otherwise}. \end{cases}$$

For position vector $\boldsymbol{x}$ and time t. Material m_{rigid} is defined as the region where $\phi_{m_{\text{rigid}}} > 0$ and the domain of material m_{fluid} as the region where $\phi_{m_{\text{fluid}}} > 0$ and $\phi_{m_{\text{rigid}}} < 0$. m_{ghost} indicates the region in which the fluid level set is extended through the rigid body.

Governing Equations 2

The interface level set, $\phi_{m1,m2}$, represents the interface between materials m_1 and m_2

$$\phi_{m_1,m_2}(\boldsymbol{x},t) = \begin{cases} > 0 & \boldsymbol{x} \in \text{material } m_1, \\ < 0 & \boldsymbol{x} \in \text{material } m_2, \\ = 0 & \text{for } \boldsymbol{x} \text{ along } (m_1, m_2) \text{ interface.} \end{cases}$$

Where needed, we obtain the interfacial level sets from the involved material level sets as

$$\phi_{m_1,m_2} = \frac{\phi_{m_1} - \phi_{m_2}}{2}.$$

The associated normal $\boldsymbol{n}$ and curvature κ for the level set functions are defined as

$$\boldsymbol{n}_{m_1,m_2} = \frac{\nabla\phi_{m_1,m_2}}{||\nabla\phi_{m_1,m_2}||}, \quad \kappa_{m_1,m_2} = \nabla \cdot \frac{\nabla\phi_{m_1,m_2}}{||\nabla\phi_{m_1,m_2}||}.$$

Governing Equations 3

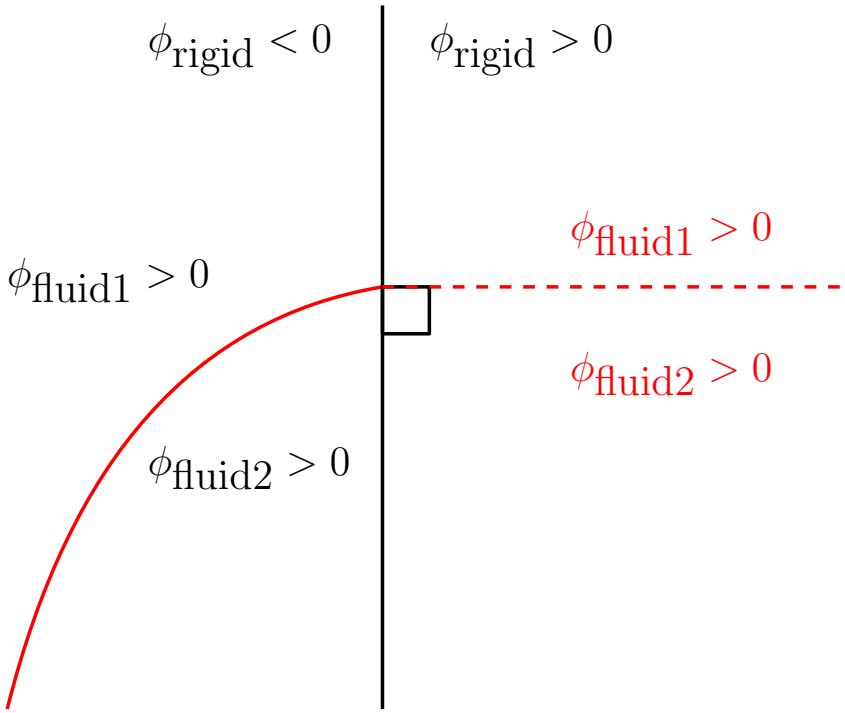

Figure: fluid level set extension through rigid region

Conservation of mass

Each fluid material, m_{fluid}, is assumed to be incompressible, so that the velocity field $\boldsymbol{u}$ is divergence free within each fluid material:

$$\nabla \cdot \boldsymbol{u} = 0.$$

To account for phase change and mass sources/sinks:

$$\nabla \cdot \boldsymbol{u} = \sum_{\text{sources}} \frac{\dot{m}_{\text{source}}}{\rho_{\text{source}}} \delta(\phi_{m_{\text{source}}}) - \sum_{\text{sinks}} \frac{\dot{m}_{\text{sink}}}{\rho_{\text{sink}}} \delta(\phi_{m_{\text{sink}}})$$

Where

$$\delta(\phi) = H'(\phi), \text{ where } H(\phi) = \begin{cases} 1 & \phi > 0 \\ 0 & \phi \leq 0. \end{cases}$$

and mass flux

$$\dot{m} = \frac{k_l \nabla T_l \cdot \boldsymbol{n}_{l,v} - k_v \nabla T_v \cdot \boldsymbol{n}_{l,v}}{L},$$

k_l, k_v: thermal conductivities of the liquid and ambient vapor regions. ρ_l, ρ_v : densities of the liquid and ambient vapor regions. L : latent heat of vaporization. $\boldsymbol{n}_{l,v}$: interface normal pointing from the vapor region into the liquid.

Conservation of momentum, energy

For each material in its domain $\phi_m(\boldsymbol{x}, t) > 0$,

Conservation of momentum:

$$(\boldsymbol{u}\rho_m)_t + \nabla \cdot (\boldsymbol{u} \otimes \boldsymbol{u}\rho_m + p_m \mathbb{I}) = \nabla \cdot (2\mu_m \mathbb{D}) + \rho_m \boldsymbol{g}(1 - \alpha_m(T_m - T_{0m})).$$

Conservation of energy:

$$(\rho_m C_{p,m} T_m)_t + \nabla \cdot (\boldsymbol{u}\rho_m C_{p,m} T_m) = \nabla \cdot (k_m \nabla T_m) \quad \text{if} \quad \phi_m(\boldsymbol{x}, t) > 0,$$

ρ_m : density, p_m : pressure, T_m : temperature, α_m : coefficients of thermal expansion, μ_m: viscosity. $\boldsymbol{g}$: acceleration due to gravity, $C_{p,m}$: heat capacity, k_m : thermal conductivity, $\mathbb{D} = \frac{1}{2}(\nabla \boldsymbol{u} + (\nabla \boldsymbol{u})^T)$ is the rate of deformation tensor.

Interfacial jump conditions

The deforming interface undergoing phase change is defined as

$$\phi_{m_s,m_d} + \boldsymbol{u}_{m_s} \cdot \nabla \phi_{m_s,m_d} = -\frac{\dot{m}}{\rho_s} ||\nabla \phi_{m_s,m_d}||$$

$$\phi_{m_d,m_s} + \boldsymbol{u}_{m_s} \cdot \nabla \phi_{m_d,m_s} = \frac{\dot{m}}{\rho_s} ||\nabla \phi_{m_d,m_s}||$$

For the velocity, pressure, and temperature interface jump conditions:

$$\begin{aligned}
\boldsymbol{u}_{m_s} \cdot \boldsymbol{n}_{m_s,m_d} - \boldsymbol{u}_{m_d} \cdot \boldsymbol{n}_{m_s,m_d} &= \dot{m} \left(\frac{1}{\rho_{m_d}} - \frac{1}{\rho_{m_s}} \right), \\
(p_{m_s} \mathbb{I} - p_{m_d} \mathbb{I}) \cdot \boldsymbol{n}_{m_s,m_d} &= -\sigma_{m_s,m_d} \kappa_{m_s,m_d} \boldsymbol{n}_{m_s,m_d} \\
&\quad + (2\mu_{m_s} \mathbb{D}_{m_s} - 2\mu_{m_d} \mathbb{D}_{m_d}) \cdot \boldsymbol{n}_{m_s,m_d}, \\
T_{m_s} &= T_{m_d}.
\end{aligned}$$

m_s : 'source' material, m_d : 'destination' material, σ_{m_s,m_d} : prescribed surface tension, κ_{m_s,m_d} : interface curvature.

Triple point junction

At a triple point, a three-phase equilibrium (Neumann's triangle) determines the contact angles for a steady state, dependent on the surface tension of the phases in contact.

$$\frac{\sin(\theta_1)}{\sigma_{23}} = \frac{\sin(\theta_2)}{\sigma_{13}} = \frac{\sin(\theta_3)}{\sigma_{12}}.$$

Numerical Method

Discretization, MAC grid:

$$\Omega_{i,j} = \left\{ \boldsymbol{x} : x \in \left[x_i - \frac{\Delta x}{2}, x_i + \frac{\Delta x}{2} \right], y \in \left[y_j - \frac{\Delta y}{2}, y_j + \frac{\Delta y}{2} \right] \right\}$$

Level sets, volume fractions, centroids, temperature, and pressure stored at cell centers. Velocities on cell faces.

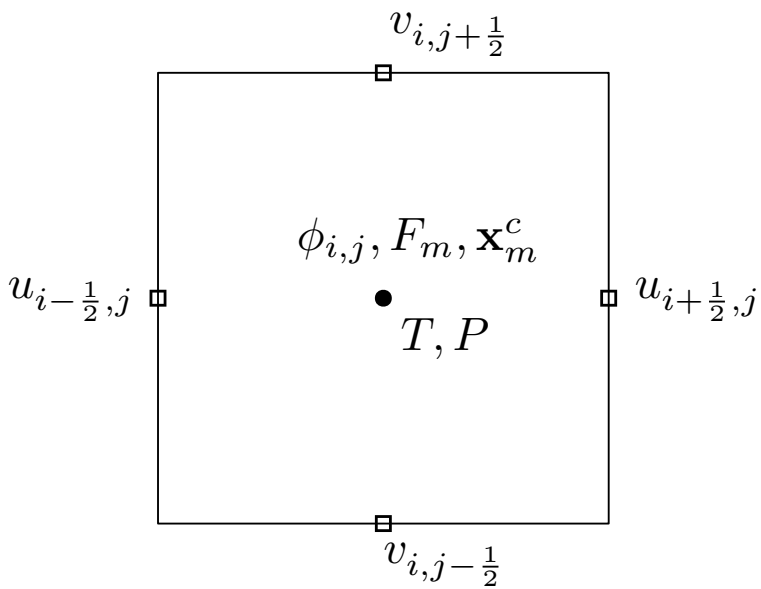

Interface Reconstruction

- coupled level set moment-of-fluid (MOF)
- continuous moment-of-fluid (CMOF)
- particle level set moment-of-fluid (PLSMOF)

moment-of-fluid (MOF)

Volume fraction F and centroid position $\boldsymbol{x}_m^c$ of material m:

$$F^n_{m,(i,j,k)} = \frac{\int_{\Omega^n_{m,(i,j,k)}} \mathrm{d}\Omega}{V_{i,j,k}}, \qquad \boldsymbol{x}^{c,n}_{m,(i,j,k)} = \frac{\int_{\Omega^n_{m,(i,j,k)}} \boldsymbol{x}\ \mathrm{d}\Omega}{V^n_{m,(i,j,k)}},$$

Cell volume $V_{i,j,k} = \int_{\Omega_{i,j,k}} \mathrm{d}\Omega,$

volume of material portion $V^n_{m,(i,j,k)} = \int_{\Omega^n_{m,(i,j,k)}} \mathrm{d}\Omega.$

MOF

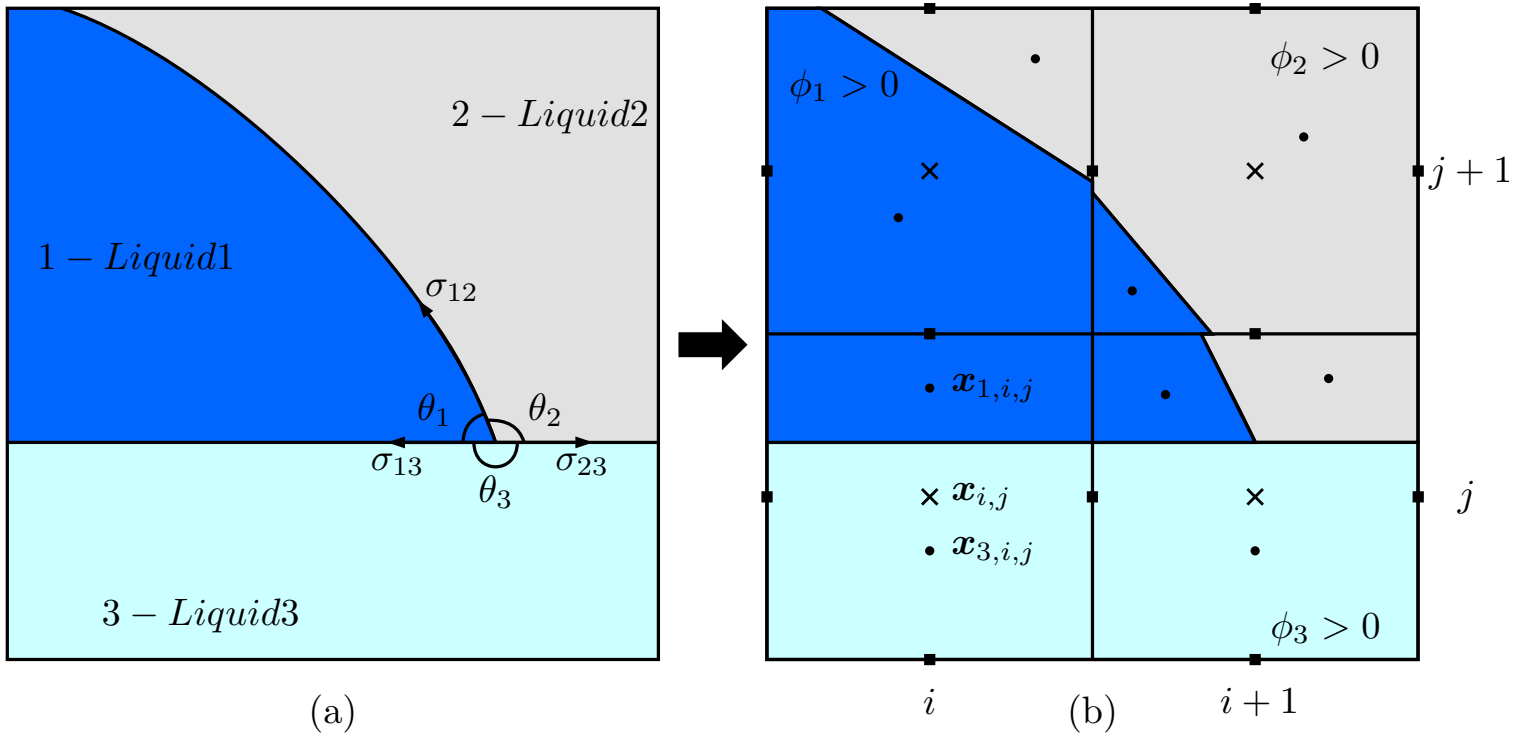

Figure: (a) Physical Domain. At the triple point, the contact angles θ are determined at equilibrium by the surface tension forces σ.
(b) Discretized Domain. $\times$: cell centers, $\bullet$: cell centroids, $\blacksquare$: MAC velocities

MOF interface reconstruction

We consider a linear interface reconstruction of the form $\boldsymbol{n} \cdot (\boldsymbol{x} - \boldsymbol{x}_{i,j}) + b = 0$.
The advected volume fraction and centroid are set as the 'reference'

$$F_{\text{ref}} \equiv F^n_{m,(ijk)}, \qquad \boldsymbol{x}^c_{\text{ref}} \equiv \boldsymbol{x}^n_{m,(ijk)}$$

The reconstructed centroid $\boldsymbol{x}^c_{\text{act}}(\boldsymbol{n}, b)$ is then found such that its error with respect to $\boldsymbol{x}^c_{\text{ref}}$ is minimized using the cost function

$$E_{\text{MOF}} = \|\boldsymbol{x}^c_{\text{ref}} - \boldsymbol{x}^c_{\text{act}}(\boldsymbol{n}, b)\|_2$$

Subject to the constraint

$$F_{\text{act}}(\boldsymbol{n}, b) = F_{\text{ref}}.$$

The slope $\boldsymbol{n}$ is obtained by the Gauss-Newton algorithm. Then a hybrid bisection/Newton method is then used to find the associated intercept b that satisfies the constraint.
(Alternatively, the intercept can be obtained analytically from the slope using Lemoine et al's method [8, 11]).

MOF

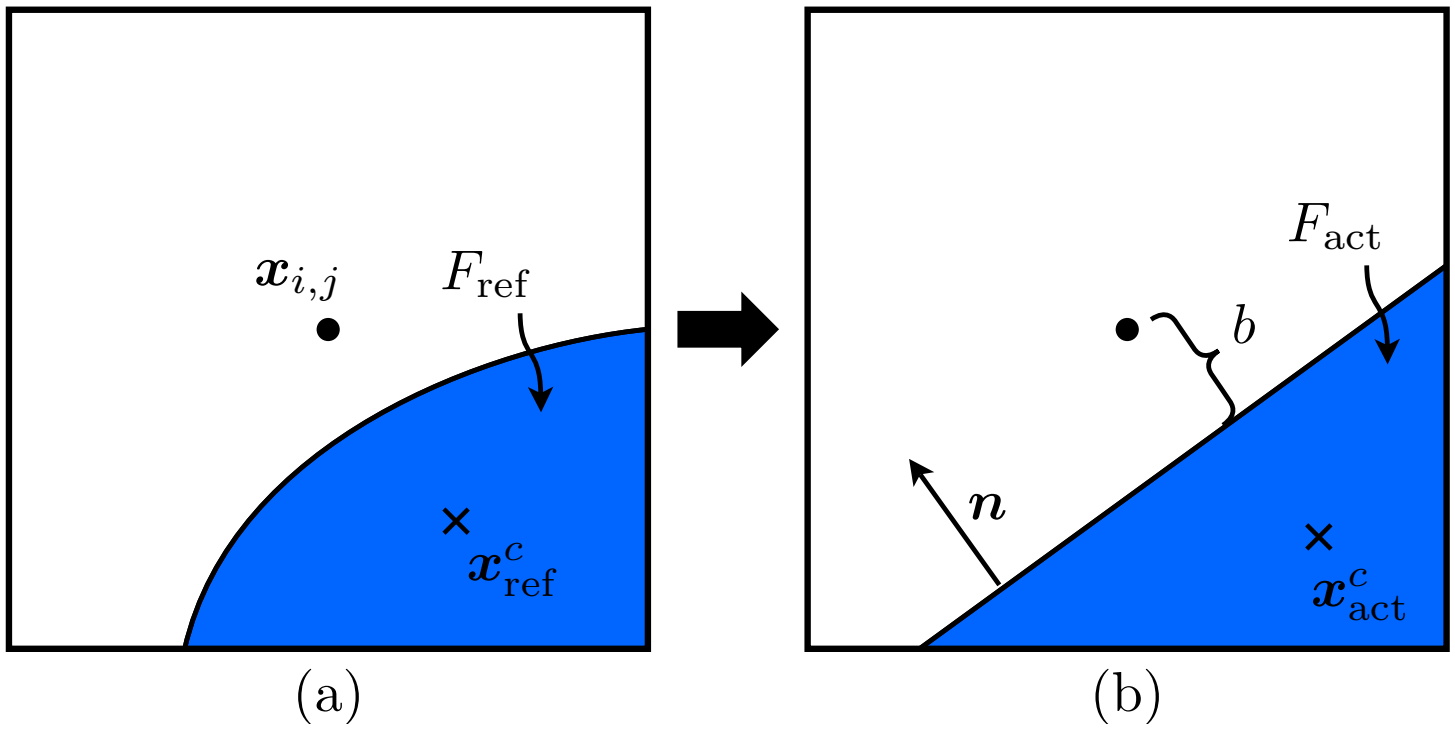

Figure: (a) Material domain in a cell $\Omega_{i,j}$, a single phase shown in blue corresponding with reference volume F_{ref} and centroid $\boldsymbol{x}^c_{\text{ref}}$.
(b) The piecewise linear MOF reconstruction. The line segment for the reconstructed volume can be represented as $\Omega_{i,j} \cap \{\boldsymbol{x} | \boldsymbol{n} \cdot (\boldsymbol{x} - \boldsymbol{x}_{i,j}) + b = 0\}$.

Nested dissection volume tesselation

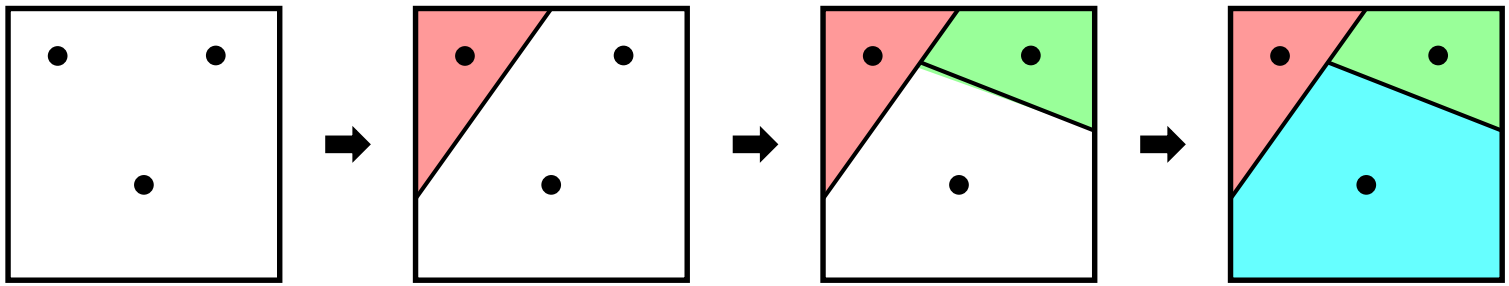

Figure: MOF reconstruction, volume-tessellation (nested dissection) procedure. Points indicate centroids, white space is the unoccupied region, and zones of color indicate reconstructed materials.

continuous moment-of-fluid (CMOF)

A supercell $\Omega^s_{i,j}$ is defined about center cell $\boldsymbol{x}_{i,j} = \{x_i, y_j\}$

$$\Omega^s_{i,j} = \left\{ \boldsymbol{x} : x \in \left[x_i - \frac{3\Delta x}{2}, x_i + \frac{3\Delta x}{2} \right], \quad y \in \left[y_i - \frac{3\Delta y}{2}, y_i + \frac{3\Delta y}{2} \right] \right\}$$

with volume fraction and centroid

$$F^{s,n}_{m,i,j} = \frac{\sum_{i'=-1}^{1} \sum_{j'=-1}^{1} F^n_{m,i+i',j+j'} V_{i+i',j+j'}}{\sum_{i'=-1}^{1} \sum_{j'=-1}^{1} V_{i+i',j+j'}}$$

$$\boldsymbol{x}^{c,s,n}_{m,i,j} = \frac{\sum_{i'=-1}^{1} \sum_{j'=-1}^{1} F^n_{m,i+i',j+j'} \boldsymbol{x}^{c,n}_{m,i+i',j+j'} V_{i+i',j+j'}}{\sum_{i'=-1}^{1} \sum_{j'=-1}^{1} F^n_{m,i+i',j+j'} V_{i+i',j+j'}}.$$

CMOF supercell

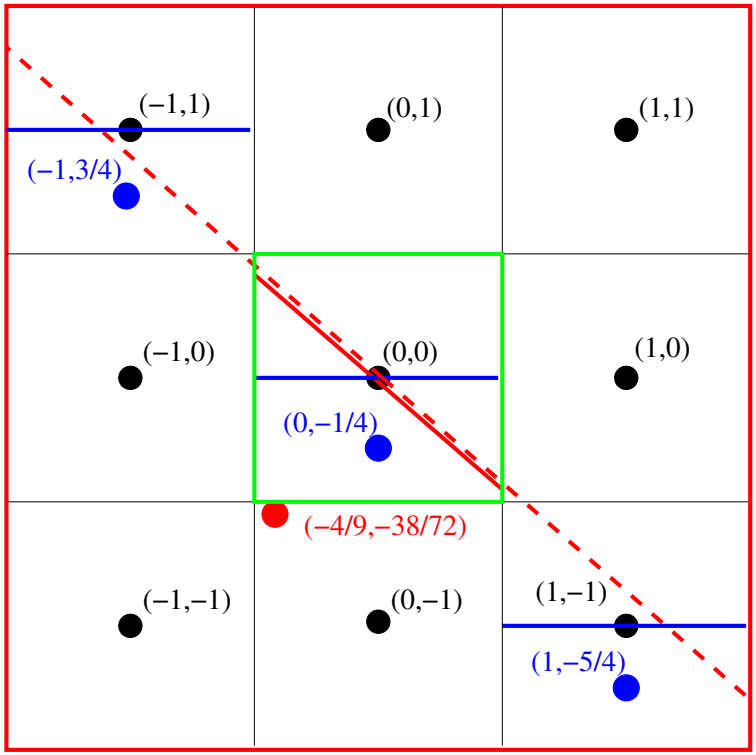

Figure: Black dots : cell centroids, blue dots : 'material 1' centroids, red dot : CMOF 'material 1' supercell centroid.

CMOF interface reconstruction

The CMOF method is then to obtain the optimal slope $\boldsymbol{n}$ and intercept b such that the following minimization problem is satisfied:

$$E_{\text{CMOF}} = \|\boldsymbol{x}_{\text{ref}}^{c,s} - \boldsymbol{x}_{\text{act}}^{c,s}(\boldsymbol{n}, b)\|_2$$

with the associated constraint

$$F_{\text{act}}(\boldsymbol{n}, b) = F_{\text{ref}}.$$

The reference volume fraction corresponds to the center cell MOF volume fraction, $F_{\text{ref}} \equiv F_{m,i,j}^{n}$, and the reference centroid is that of the supercell, $\boldsymbol{x}_{\text{ref}}^{c} \equiv x_{\text{m,i,j}}^{c,s,n}$. (i.e. find the slope that minimizes the distance between the supercell and CMOF centroid, subject to the constraint that the center cell's volume fraction must match the original volume fraction.

Either Gauss-Newton or machine-learning decision tree to find slope.

particle level set moment-of-fluid (PLSMOF)

The linear reconstructed distance function is given by the form

$$\hat{\phi} = \boldsymbol{n} \cdot (\boldsymbol{x} - \boldsymbol{x}_0) + \hat{b}$$

Where $\boldsymbol{n}$ and $\hat{b}$ are found such that they minimize the following cost function:

$$C(\boldsymbol{n}, \hat{b}) = \sum_{p \in \text{stencil}} w_p (\hat{\phi}(\boldsymbol{n}, \hat{b}) - \phi_p)^2 + \sum_{i,j,k \in \text{stencil}} w_{ijk} (\hat{\phi}(\boldsymbol{n}, \hat{b}) - \phi_{i,j,k})^2$$

ϕ_{ijk} : cell-centered level set value, ϕ_p : particle level set value, 'stencil' is defined as a $3 \times 3 (\times 3)$ stencil about the evaluated cell Ω_0. The weights, $w_{i,j,k}$ and w_p are inversely proportional to the distance from the center point, defined here as

$$w_{ijk} = wx_{ijk} * wy_{ijk} * wz_{ijk} * \delta_{\text{smooth}}(\phi_{ijk}), \qquad w_p = w^{\text{dim}} * \delta_{\text{smooth}}(\phi_p)$$

PLSMOF interface reconstruction

1	12	1
12	12^2	12
1	12	1

$$\begin{cases} wx_{ijk} = \begin{cases} 12, & i = 0 \\ 1, & i = 1 \text{ or } -1 \end{cases} \\ wy_{ijk} = \begin{cases} 12, & j = 0 \\ 1, & j = 1 \text{ or } -1 \end{cases} \\ wz_{ijk} = \begin{cases} 12, & k = 0 \\ 1, & k = 1 \text{ or } -1 \end{cases} \end{cases}, \qquad w = \begin{cases} 12, & d < \Delta x \\ 1, & d \geq \Delta x \end{cases}$$

$$\delta_{\text{smooth}} = \begin{cases} 0, & \phi \geq \varepsilon \text{ or } \phi \leq -\varepsilon \\ \frac{1}{2\varepsilon}\left(1 + \cos\left(\frac{\pi\phi}{\varepsilon}\right)\right), & \text{otherwise} \end{cases}$$

$d = ||x_p - x_0||$: distance between particle and stencil center, $\varepsilon = \sqrt{\text{dim}}\ \Delta x$.

$C(\boldsymbol{n}, \hat{b})$ is minimized by a least squares approach, finding the the optimal slope $\boldsymbol{n}$ and intercept $\hat{b}$ for the involved particles.
In order to agree with the existing volume reconstruction. $\hat{b}$ is replaced by b, found by hybrid bisection/Newton method, such that the volume fraction is satisfied for the new slope.

PLSMOF particle addition/deletion

For each computational cell $\Omega_{i,j,k}$,

- if the cell contains an interface, subdivide uniformly into N^{dim} pieces
- if the subdivision doesn't already contain a particle
  - seed particle at subdivision center (interpolate LS and assign particle ϕ_p and material m)
  - if subdivision contains interface, seed particle directly on interface ($x^{\text{cp}} = x_{\text{sub}} - \phi_{m,p}(x_p)\boldsymbol{n}_{m,p}$)
- if the subdivision contains particles
  - delete trailing particles (interface particles if $|\phi_{m,p}| > \Delta x_{\text{sub}}$, near-interface particles if $|\phi_{m,p}| > \Delta x$)
  - delete particles (closest neighbors first) if number within subcell exceeds threshold n^{delete}

PLSMOF particle seeding

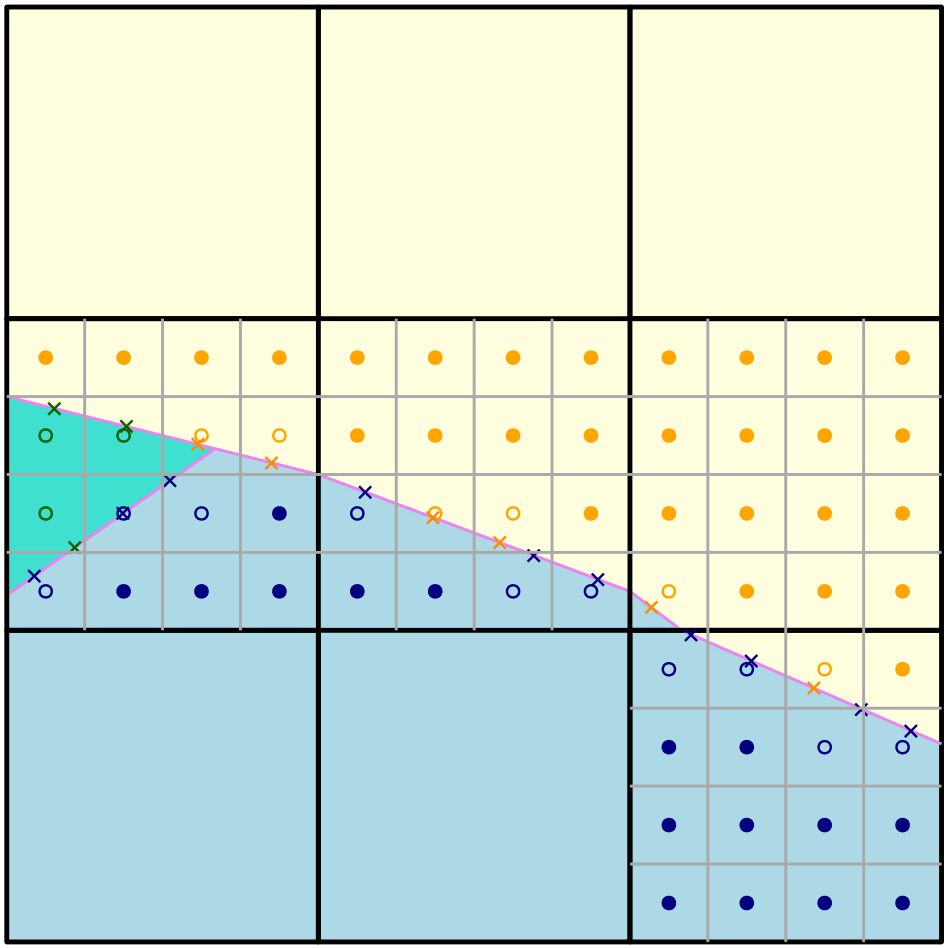

Figure: $N = 4$ subdivisions

• : near-interface particles, × : on-interface particles, ◯ : particle sent to interface, color indicates associated material

PLSMOF/MOF

If no particles are available or the least squares matrix is singular, then the Moment of Fluid reconstruction is used. Particles are seeded only on uncovered AMR regions.

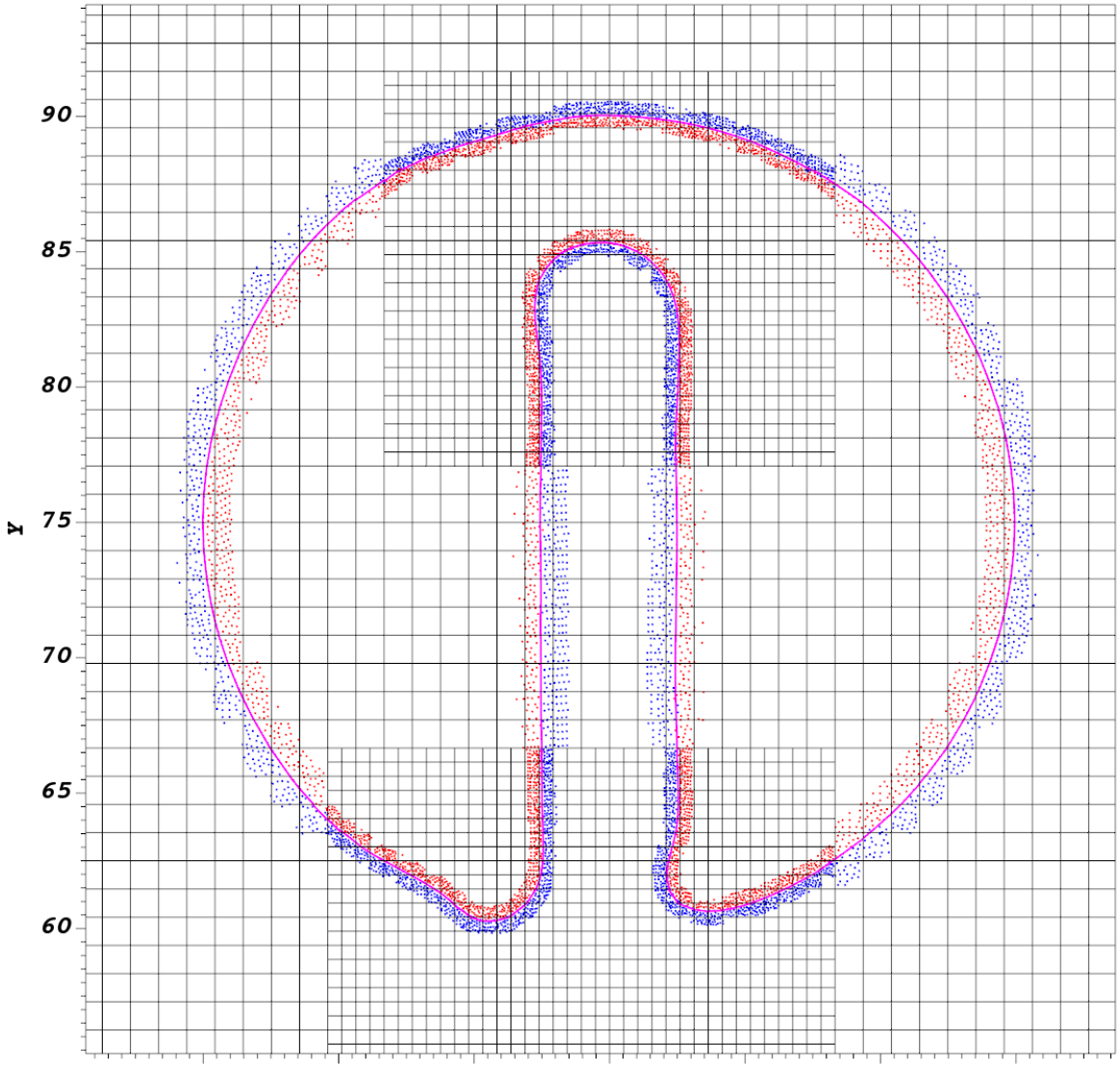

Redistancing

- Iterate over the entire computational domain
- If $F_m > 10^{-3}$, then check if $F_m > 1 - 10^{-3}$ for any surrounding cells, if so then increment local material count m.
- If more than one material is found within the cell, it is a 'support cell': cells within a $9 \times 9 (\times 9)$ neighborhood about this cell gets redistanced.

Redistancing

Redistancing level set from reconstructed interface:

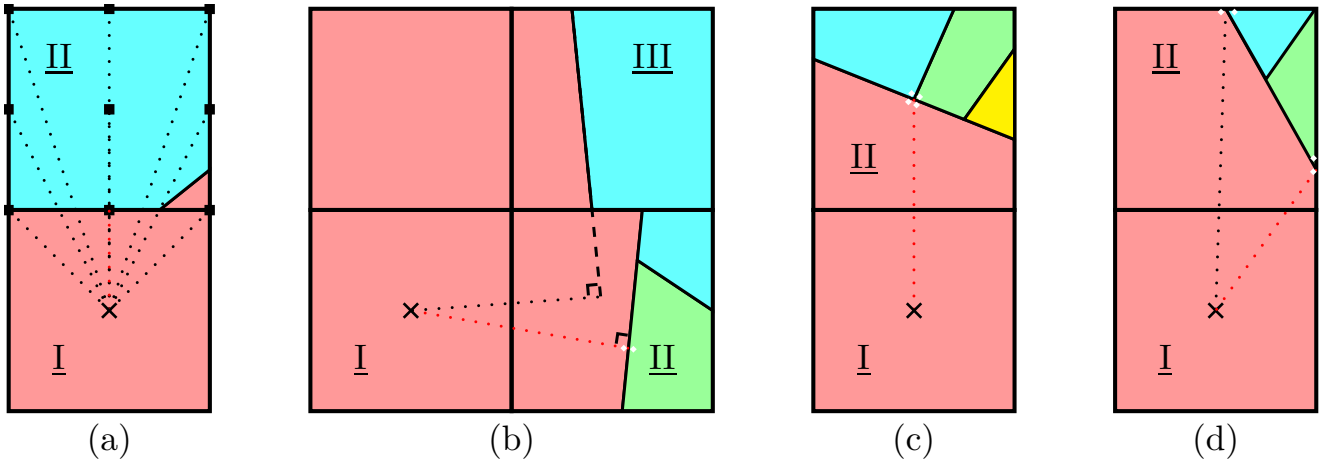

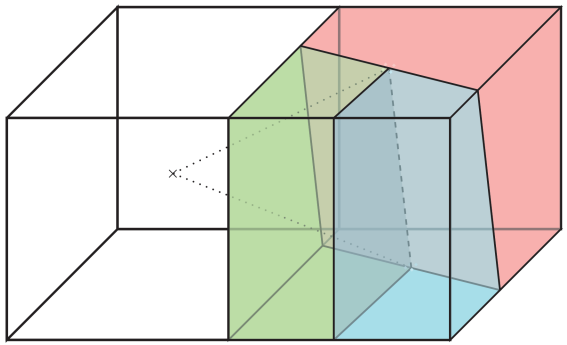

Redistancing, stencil reduction

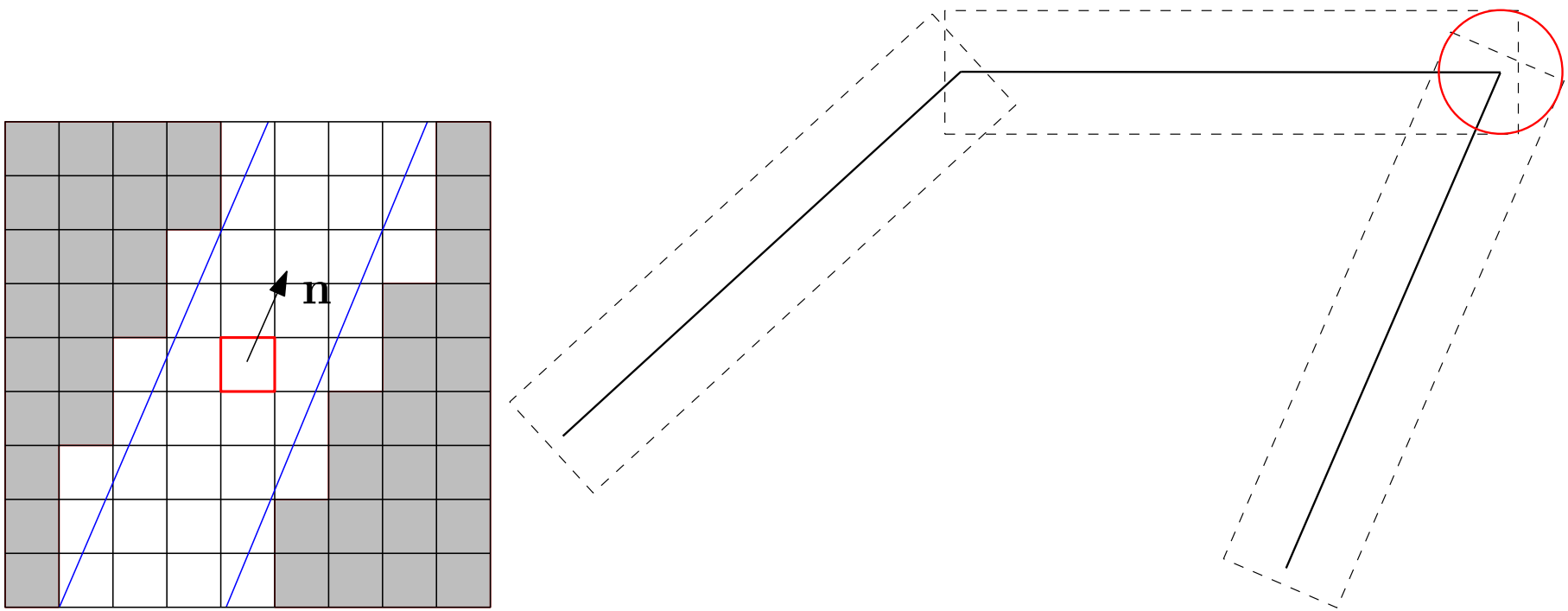

Figure: reduced stencil aligned with normal, 3 cell width
note: reduced stencil may not update all cells within narrow band

[10]

Algorithm

0. Initialize (for each material) a level set function, VOF function, centroids, velocity (on the cell center grid), density, and temperature at cell centers.

The level set function is replaced with the exact signed distance to the multimaterial MOF reconstructed interface.

Seed initial particles using the level set interface given by initial MOF reconstruction. And apply a redistancing step for the level set using the particles.

A divergence free MAC velocity is then derived from the cell centered velocity:

($t = 0$ only), we solve $\boldsymbol{u}^{\text{MAC}} = \boldsymbol{u}^{\text{cell\_to\_MAC}} - \dfrac{\nabla p}{\rho}, \quad \nabla \cdot \boldsymbol{u}^{\text{MAC}} = 0.$

Algorithm

For each timestep,
1. Directionally-split Cell Integrated Semi-Lagrangian (CISL) advection of volume fractions, centroids, level set functions, MAC velocity, cell velocity, temperature, density, particles. Note: the slope reconstruction (either MOF or particle-augmented) is performed before every CISL sweep.

2. Redistance the level set, add and delete particles.

3. Determine $\dot{m}$, T_{sat} for the rate of phase change.

4. Update the interface using unsplit advection (volume fractions, centroids, level set functions, particles). Slope reconstruction.

5. Redistance the level set, add and delete particles.

6. Determine the source terms for $\nabla \cdot \boldsymbol{u}$ equation.

Algorithm

7. Diffusion

viscosity, $\frac{\rho^{\text{mix},n+1}}{\Delta t}(\boldsymbol{u}^* - \boldsymbol{u}^{\text{advection}}) = \nabla \cdot (2\mu\mathbb{D}^*) - \rho^{n+1}(\alpha^{n+1}(T^{n+1} - T_0))\boldsymbol{g}$

thermal, $\frac{(\rho C_{p,m})^{\text{mix},n+1}}{\Delta t^{\text{swept}}}(T_m^{n+1} - T_{\text{sat},m}) = \nabla \cdot (k_m \nabla T_m^{n+1})$

8. Pressure Projection

$$\frac{\boldsymbol{u}^{n+1} - \boldsymbol{u}^*}{\Delta t} = -\frac{\nabla p^{n+1}}{\rho^{\text{MAC,mix},n+1}} + \boldsymbol{g} - \frac{\sum_{m=1}^{M} \gamma_m \kappa_m \nabla H(\phi_m)}{\rho^{\text{MAC,mix},n+1}}$$

$$\nabla \cdot \boldsymbol{u}^{n+1} = \sum_{\text{sources}} \frac{\dot{m}_{\text{source}}}{\rho_{\text{source}}} \delta(\phi_{m_{\text{source}}}) - \sum_{\text{sinks}} \frac{\dot{m}_{\text{sink}}}{\rho_{\text{sink}}} \delta(\phi_{m_{\text{sink}}})$$

$$\gamma_{m_1} = \frac{1}{2}(\sigma_{m_1,m_2} + \sigma_{m_1,m_3} - \sigma_{m_2,m_3})$$

$$\gamma_{m_2} = \frac{1}{2}(\sigma_{m_1,m_2} + \sigma_{m_2,m_3} - \sigma_{m_1,m_3})$$

$$\gamma_{m_3} = \frac{1}{2}(\sigma_{m_1,m_3} + \sigma_{m_2,m_3} - \sigma_{m_1,m_2})$$

$$\boldsymbol{u}^{n+1} = \boldsymbol{u}^* - \Delta t \frac{\nabla p^{n+1}}{\rho^{\text{MAC,mix},n+1}}$$

note:
- probe temperature depends on the interface temperature
- κ is approximated using the VOF Height Function technique
- third term in pressure projection step exhibits a strong discontinuity at the triple point

[9, 14, 15, 12]

Numerical Method

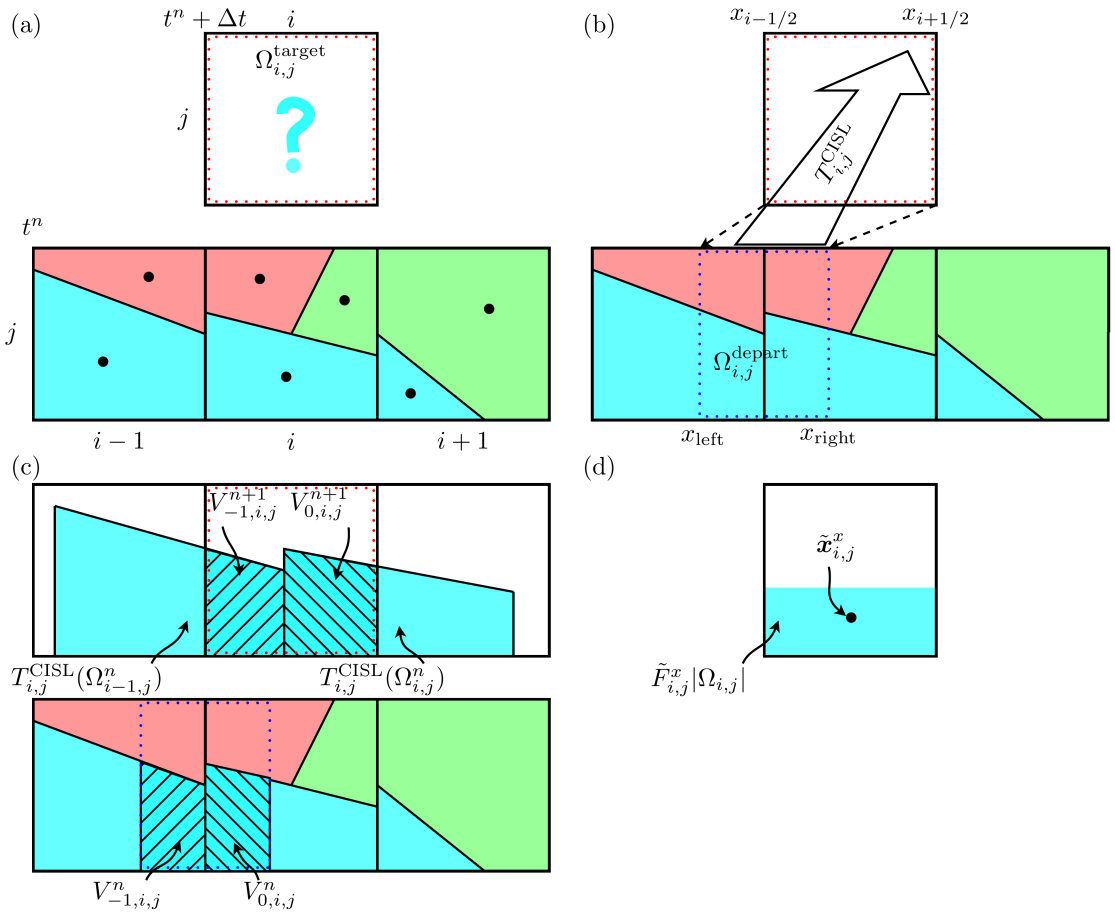

Figure: CISL-MOF method [figure from Pei et al. [13]]: find region contained by cell's backwards-traced characteristics, map to cell, update volume fraction and centroid.

Numerical Method

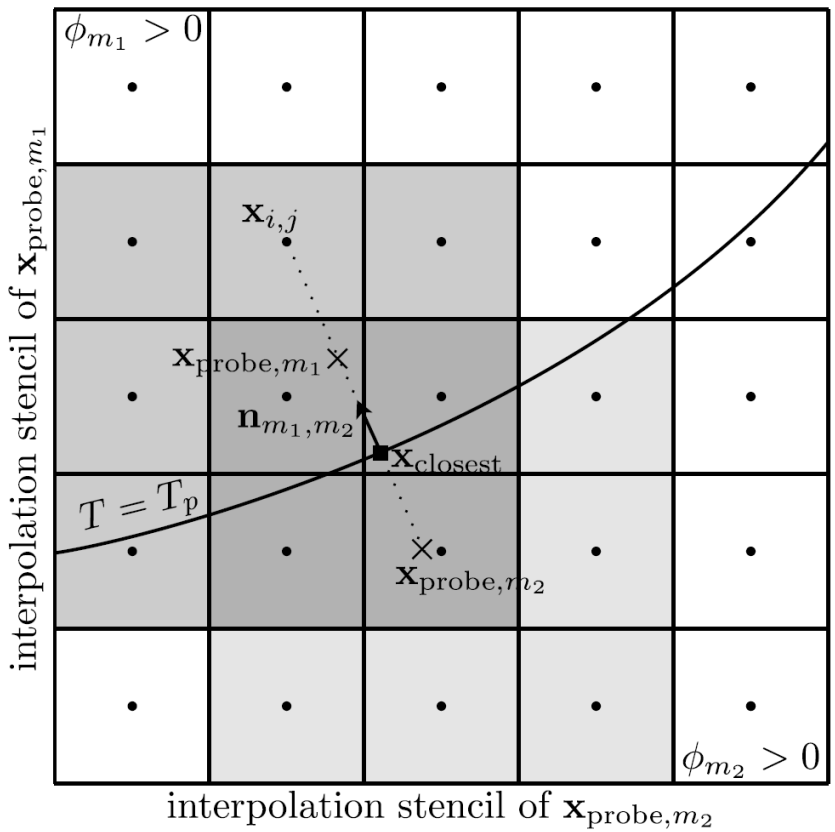

Figure: Probe temperatures [figure from Vahab et al. [15]]
The closest point is found on the interface by $x_{\text{closest}} = x_{i,j} - \phi_{m_1,m_2}\boldsymbol{n}_{m_1,m_2}$,
two probe points are extended in either normal direction and $T(x_{\text{probe}})$ is found by interpolation.
$\nabla T_{m_1} = (T_{\text{probe},m_1} - T_{\text{sat},m_1,m_2})\boldsymbol{n}_{m_1,m_2}/h$ and
$\nabla T_{m_2} = -(T_{\text{probe},m_2} - T_{\text{sat},m_1,m_2})\boldsymbol{n}_{m_1,m_2}/h$, where T_{sat} is the phase change saturation temperature.

Numerical Experiments: Split Disk

- domain: $[0, 100] \times [0, 100]$
- disk radius: 15
- material 1 : left half of disk, material 2 : right half of disk, material 3 : outside
- initial disk center: $(50, 75)$
- velocity field: $u = -(\pi/314)(y - 50), \quad v = (\pi/314)(x - 50)$
- 5 revolutions, $t_{\text{final}} = 3140$

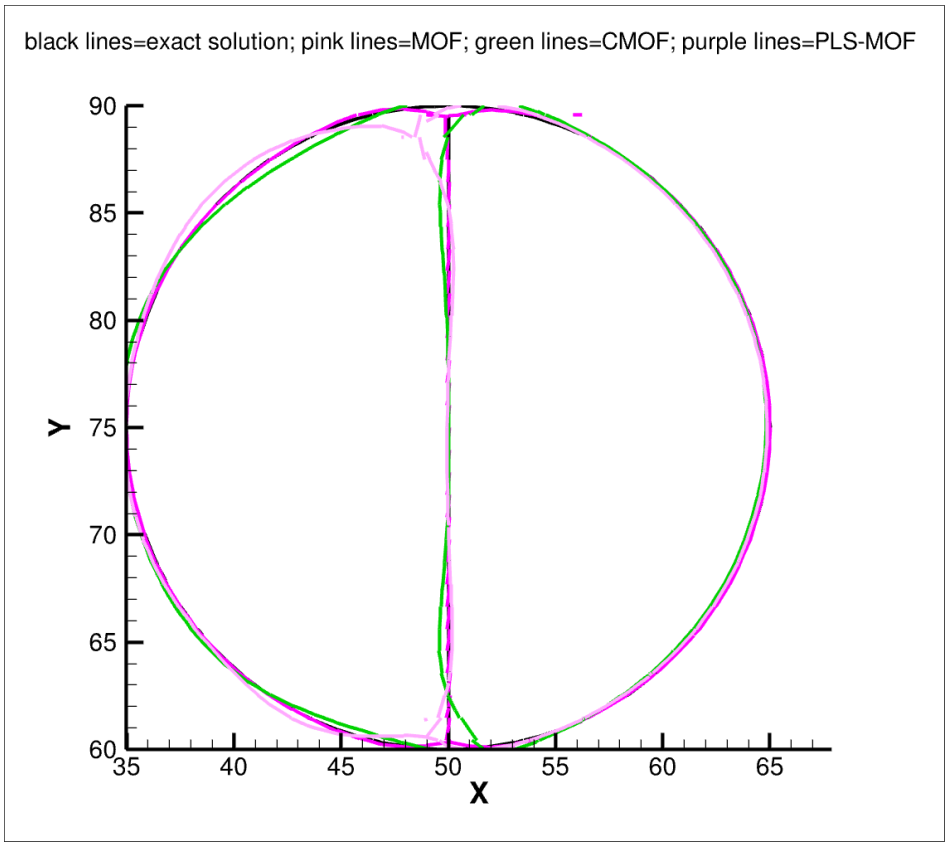

Numerical Experiments: Split Disk

Table: Comparison of the symmetric difference error
$E_{\text{sym}} = |\Omega^{\text{approx}} \cap \Omega^{\text{exact,complement}}| + |\Omega^{\text{approx,complement}} \cap \Omega^{\text{exact}}|$

	material 1	material 2	material 3
MOF	2.9	2.7	3.9
CMOF	19.3	14.0	18.9
PLSMOF	19.5	12.1	17.6

Table: Cost comparison, performance profiling times shown in seconds

MOF	reconstruction: Level set redistancing (MOF):	340 351
CMOF	reconstruction: Level set redistancing (CMOF):	1837 327
PLS-MOF	PLSMOF reconstruction: (intercept + slopes + particle advection procedures) Level set redistancing (PLSMOF):	330 329

Numerical Experiments: Stretching Liquid Lens

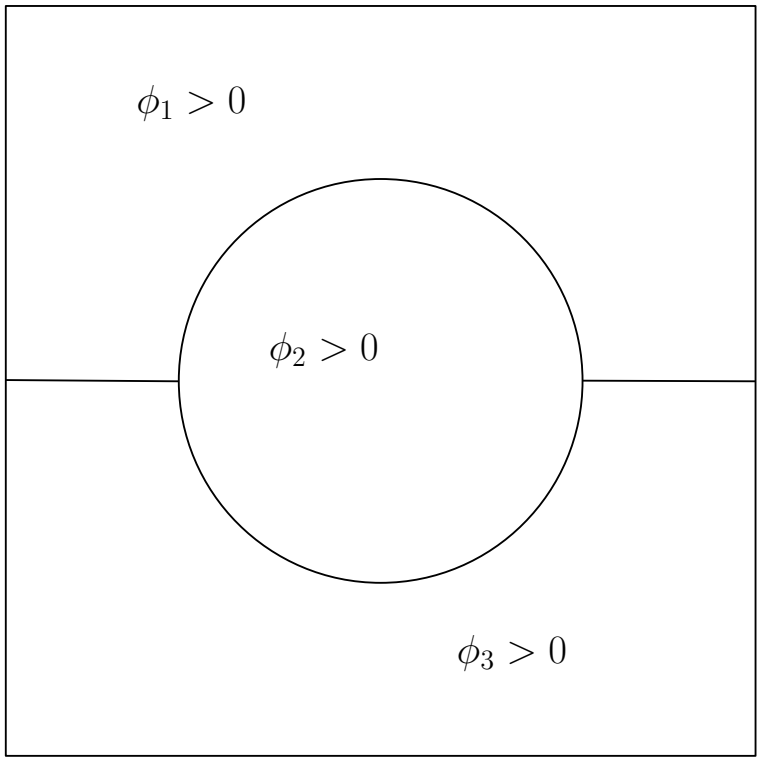

Noise intentionally added to the initial centroids:

$$\boldsymbol{x}_{\text{noise}}^{\text{ref}} = \boldsymbol{x}^{\text{ref}} + (2r-1)\Delta x, \quad (r\text{: random variable from uniform distribution } (0 \leq r \leq 1))$$

[7, 9]

Numerical Experiments: Stretching Liquid Lens

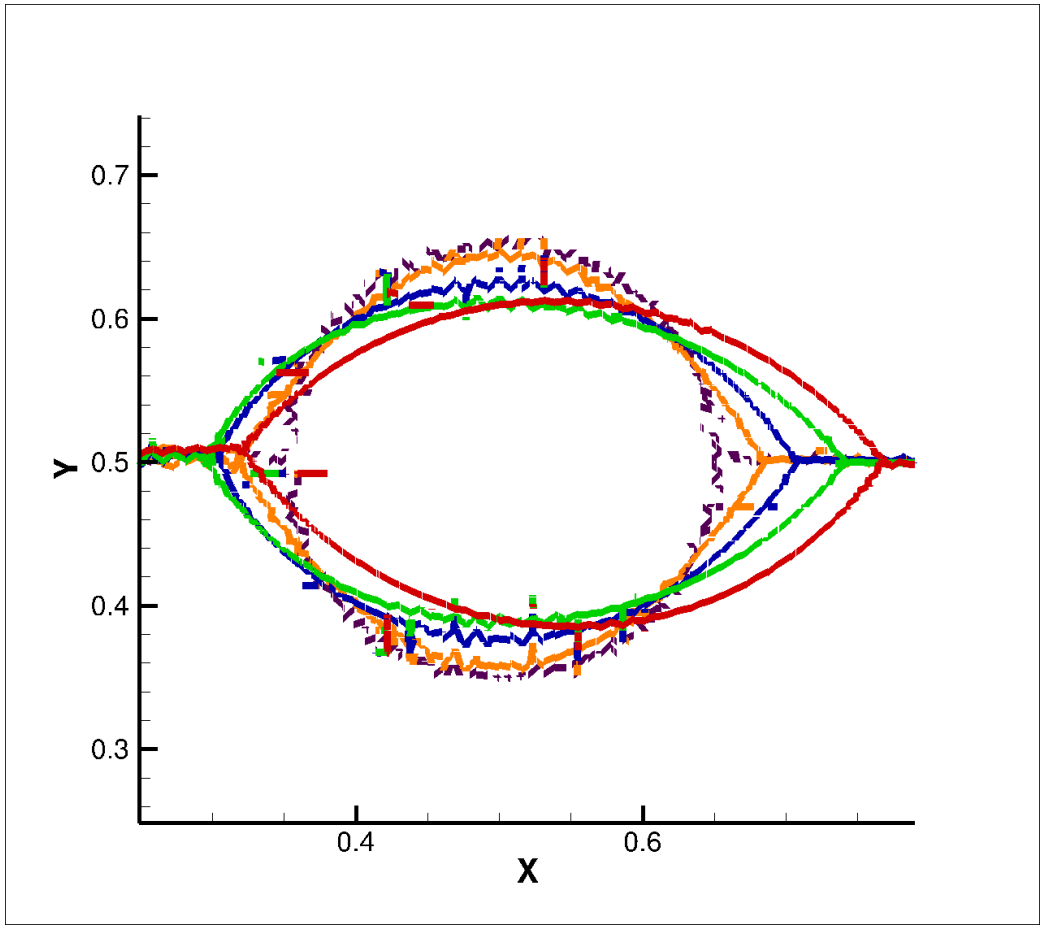

Figure: **MOF**, stretching of a liquid lens.
Times shown are: 0.0 (brown), 0.187 (orange), 0.375 (blue), 0.749 (green), and 4.0 (red).
Effective fine grid resolution : $\Delta x_{\text{fine}} = 1/128$.
Initial noise persists.

Numerical Experiments: Stretching Liquid Lens

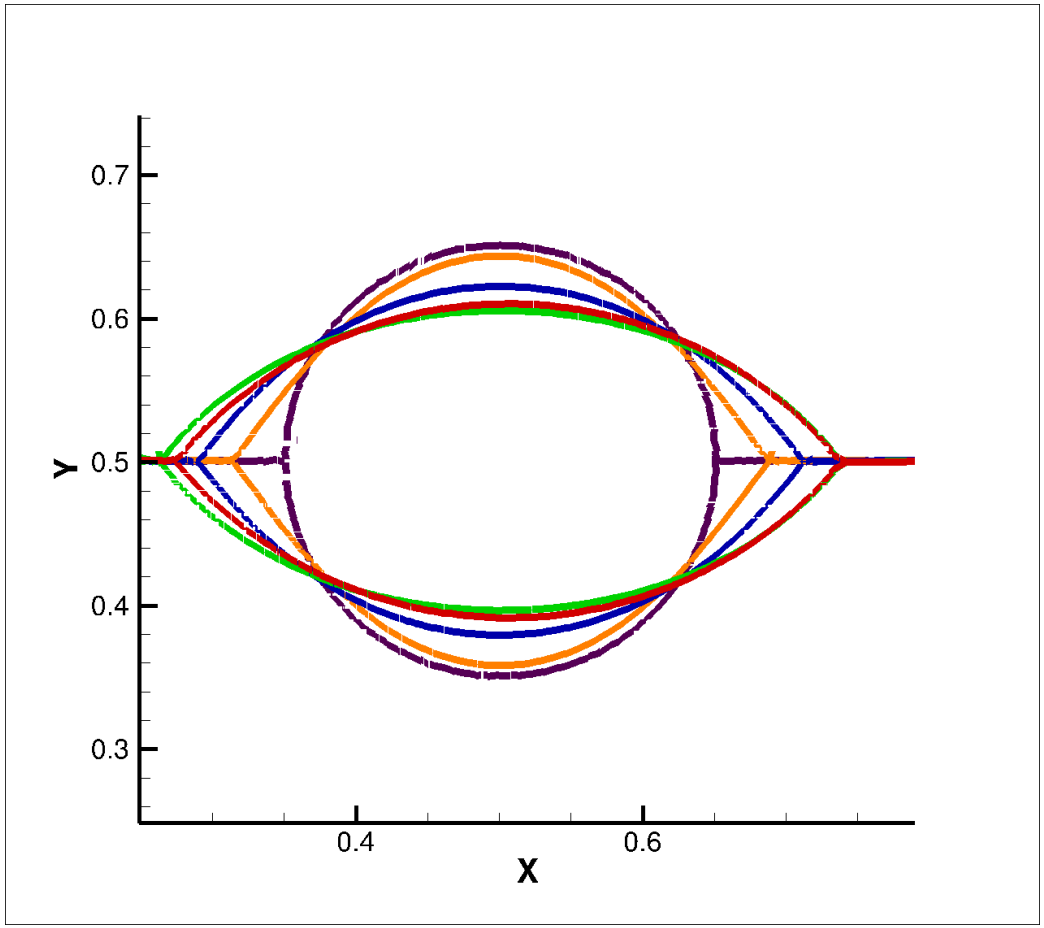

Figure: **CMOF**, stretching of a liquid lens.
Times shown are: 0.0 (brown), 0.187 (orange), 0.375 (blue), 0.749 (green), and 4.0 (red).
Effective fine grid resolution : $\Delta x_{\text{fine}} = 1/128$.
Initial noise immediately damped out.

Numerical Experiments: Stretching Liquid Lens

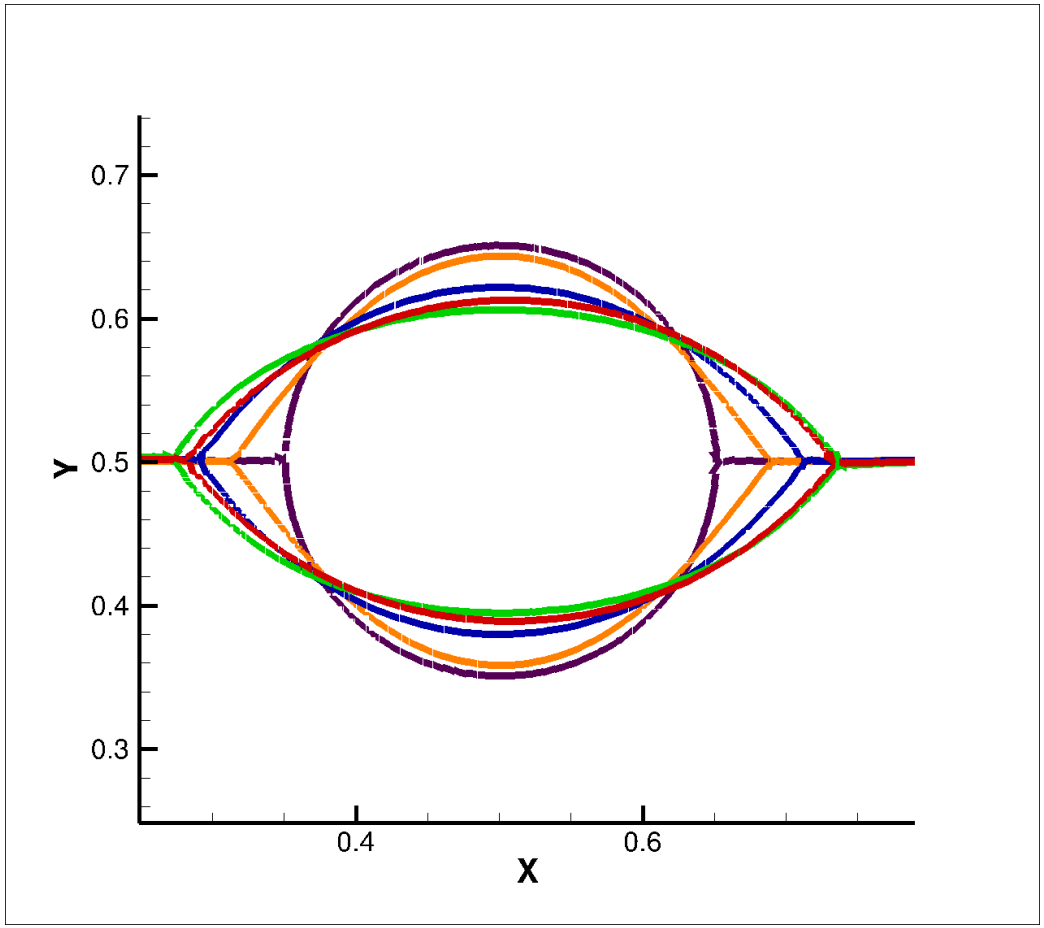

Figure: **PLSMOF**, stretching of a liquid lens.
Times shown are: 0.0 (brown), 0.187 (orange), 0.375 (blue), 0.749 (green), and 4.0 (red).
Effective fine grid resolution : $\Delta x_{\text{fine}} = 1/128$.
Initial noise immediately damped out.

Numerical Experiments: Stretching Liquid Lens

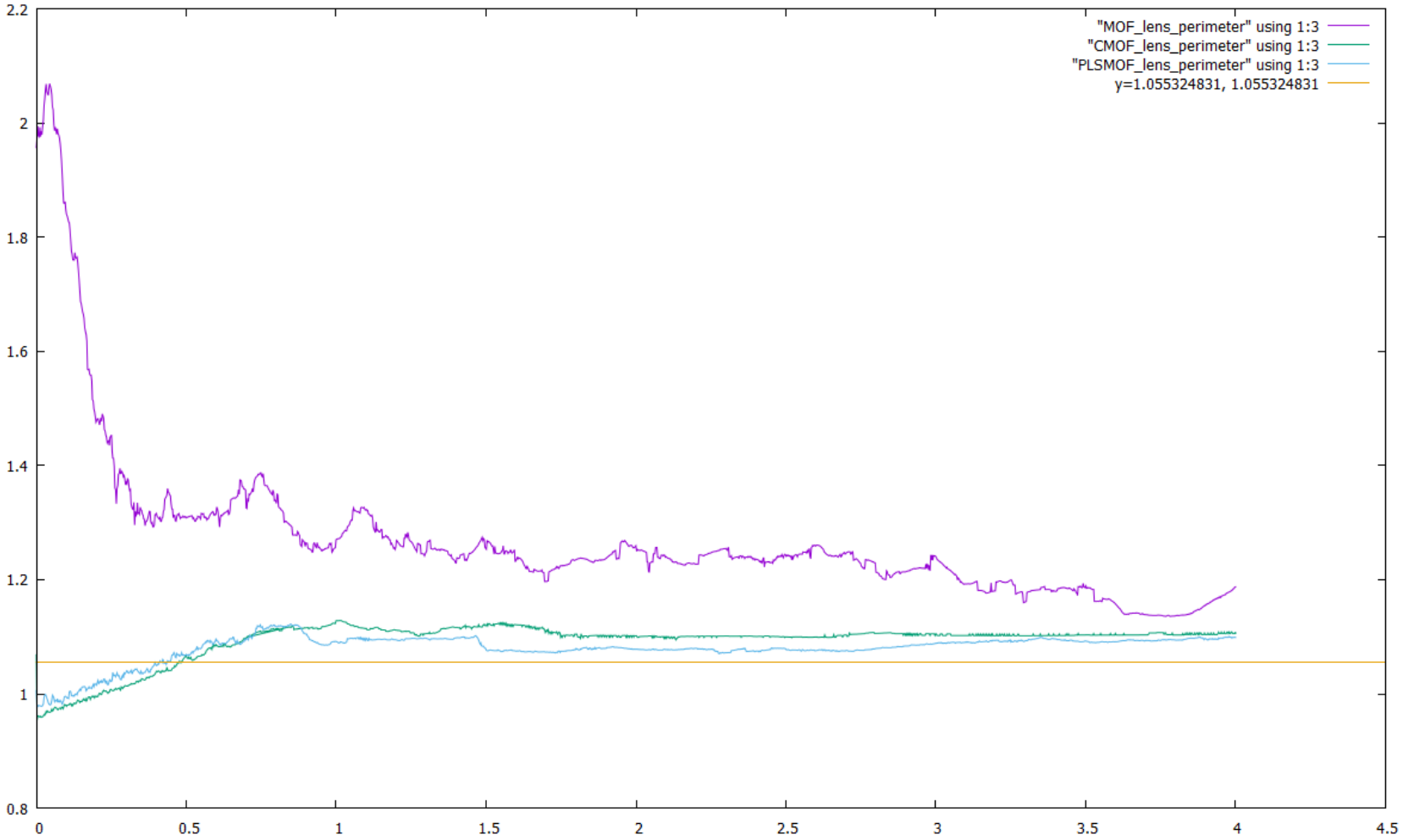

Figure: Lens perimeter vs time
purple: MOF, green: CMOF, blue: PLSMOF, orange: $\mathcal{P}_0^{\text{exact}}$.

Numerical Experiments: Freezing Droplet

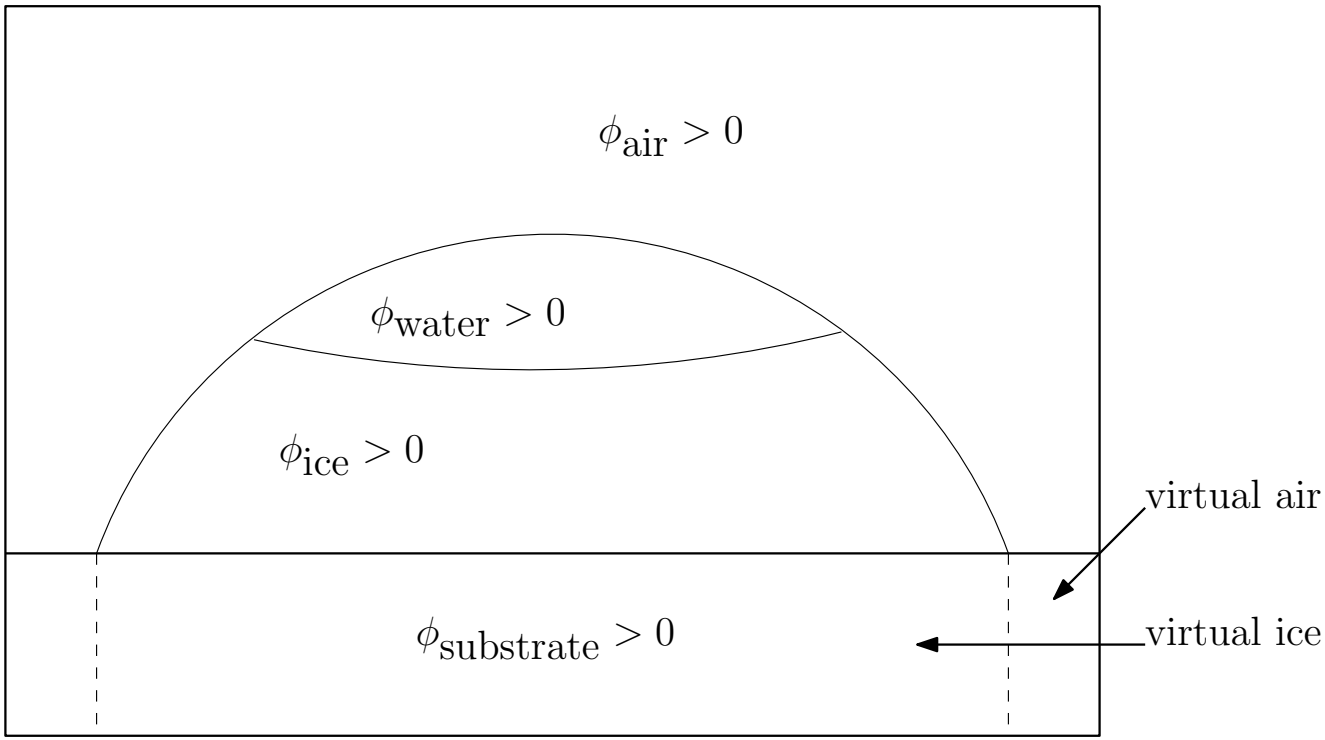

Figure: Freezing droplet on a cold substrate. Dotted line indicates fluid interface extension through rigid material.

- The substrate temperature is maintained at $-6°\text{C}$.
- The Latent Heat is $3.34\text{E}{+9}$ erg/g.
- Grid size is 128×128.

[5, 16]

Numerical Experiments: Freezing Droplet

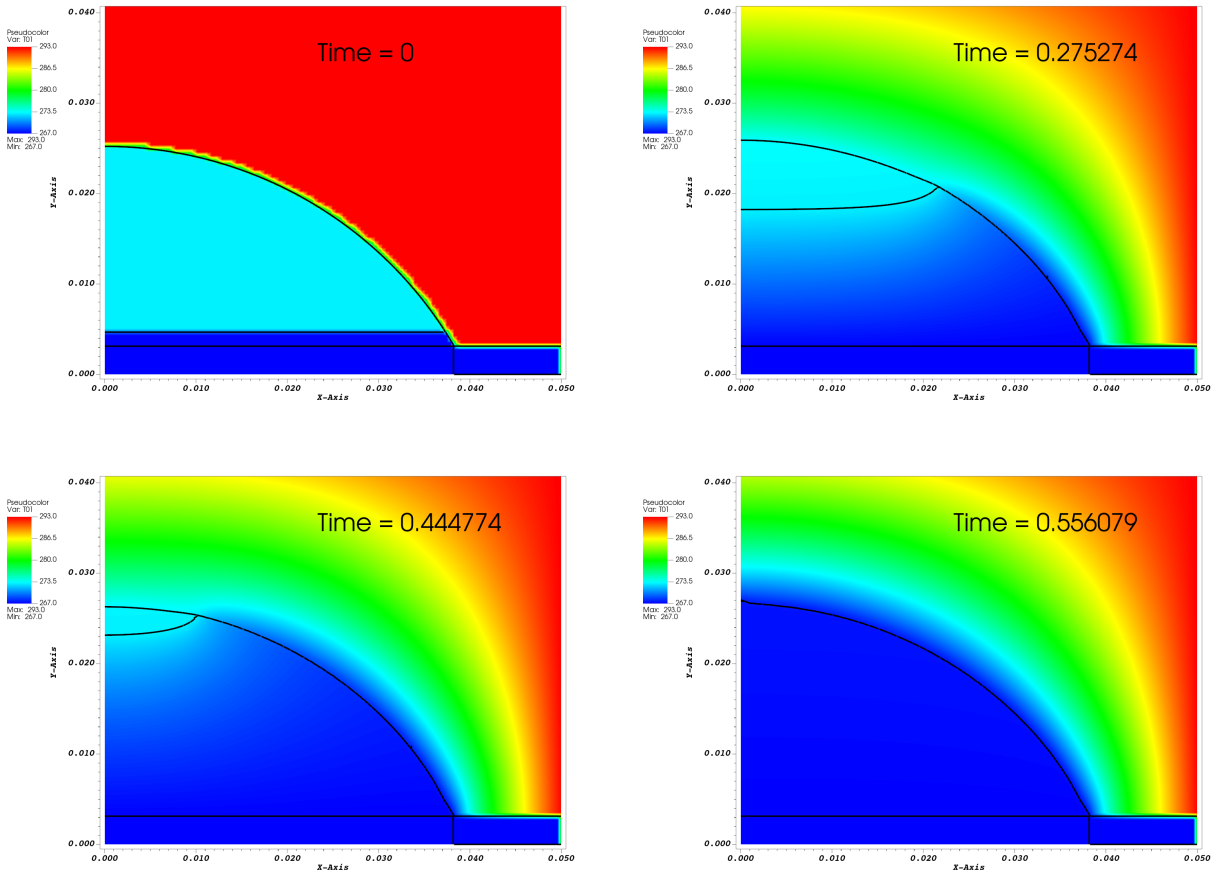

Figure: **PLSMOF**: Freezing droplet on cold substrate: liquid, gas, ice interfaces over time.

Numerical Experiments: Freezing Droplet

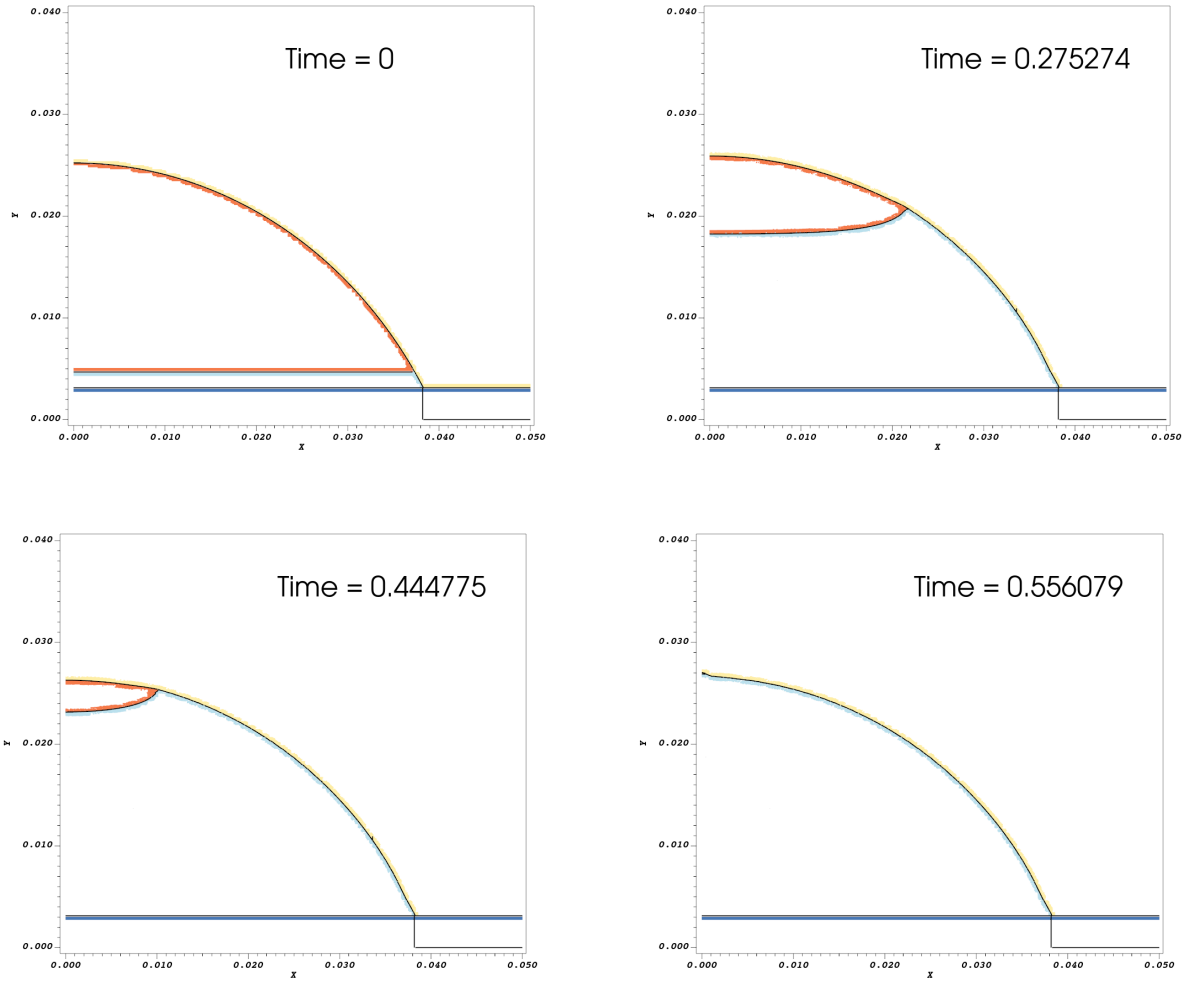

Figure: **PLSMOF**, Particles: yellow-air, orange-water, cyan-ice, blue-substrate

Numerical Experiments: Deformation of Spherical Ullage Due to Impinging Jet

Tank pressure control experiment (TPCE)[1, 2]:
A liquid jet impinges on a spherical vapor ullage in a microgravity environment.
In the TPCE experimental results [1, 2], the following behaviors were found:

- $\text{We}_j > 14$, then the jet would penetrate the bubble
- $\text{We}_j \leq 1.5$, then the vapor bubble would be propelled to the top of the tank without any breakup
- $1.5 \leq \text{We}_j \leq 14$, bubble may become asymmetric, may be propelled or pierced.

It is found in numerical experiments that a Weber number of $\text{We}_j^{\text{cutoff}} \approx 5.0$ is where the jet begins to pierce the ullage.

$$\text{We}_j = \frac{\rho_l V_0^2 R_0^2}{\sigma D_j}. \tag{1}$$

ρ_l : density of the liquid, V_0 : velocity of the liquid jet at the nozzle, R_0 : nozzle radius, σ : coefficient of surface tension for the liquid/vapor interface, and D_j : diameter of the jet where it impinges the vapor region.

Numerical Experiments: Deformation of Spherical Ullage Due to Impinging Jet ($We_j = 4.875$)

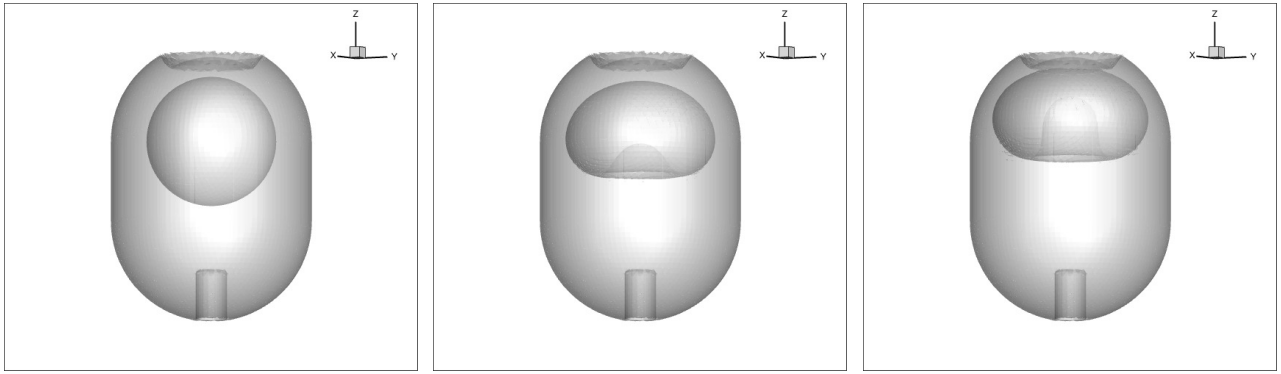

Figure: **CMOF**, deformation of a spherical ullage due to a liquid jet, $We_j = 4.875$. Times $t = 0.0$, 8.45, and 15.7 shown. The jet does not penetrate the ullage. Gridsize $64 \times 64 \times 64$.

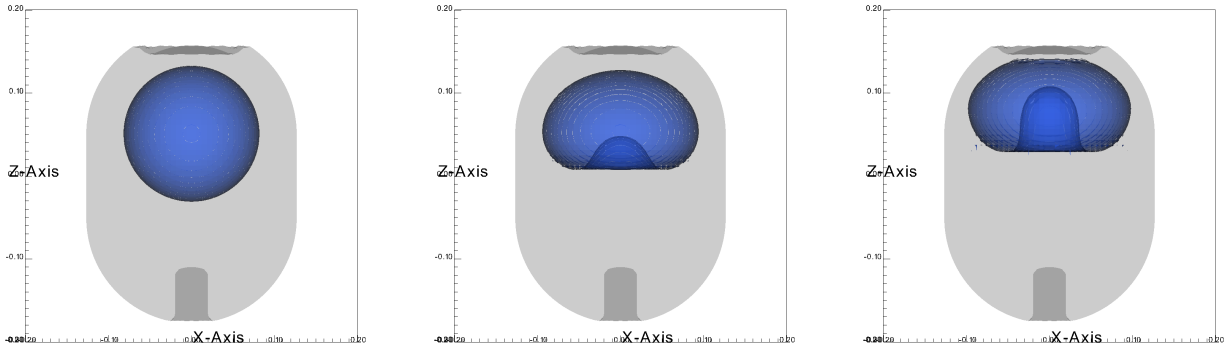

Figure: **PLSMOF**, deformation of a spherical ullage due to a liquid jet, $We_j = 4.875$. Times $t = 0.0$, 8.45, and 15.68 shown. The jet does not penetrate the ullage. Gridsize $64 \times 64 \times 64$.

Numerical Experiments: Deformation of Spherical Ullage Due to Impinging Jet ($We_j = 5.25$)

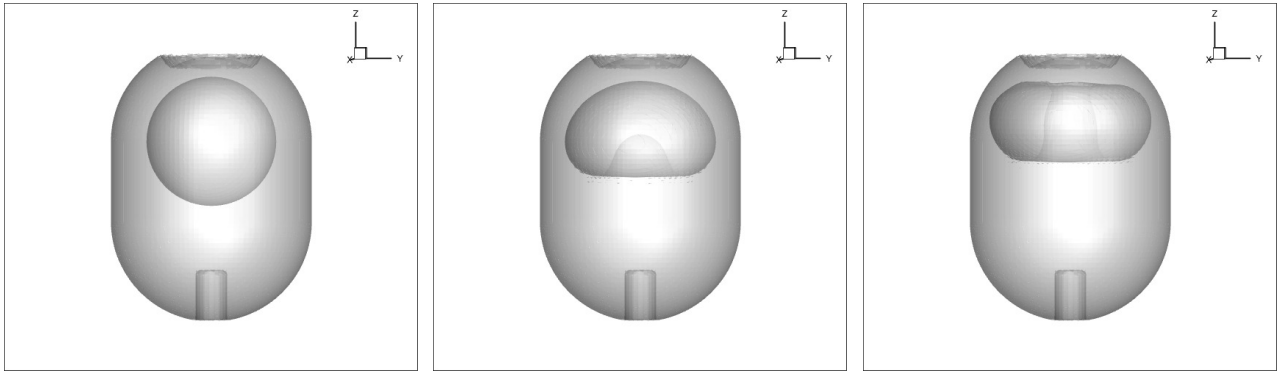

Figure: **CMOF**, deformation of a spherical ullage due to a liquid jet, $We_j = 5.25$. Times $t = 0.0$, 7.84, and 15.5 shown. The jet penetrates the ullage. Grid size was $64 \times 64 \times 64$.

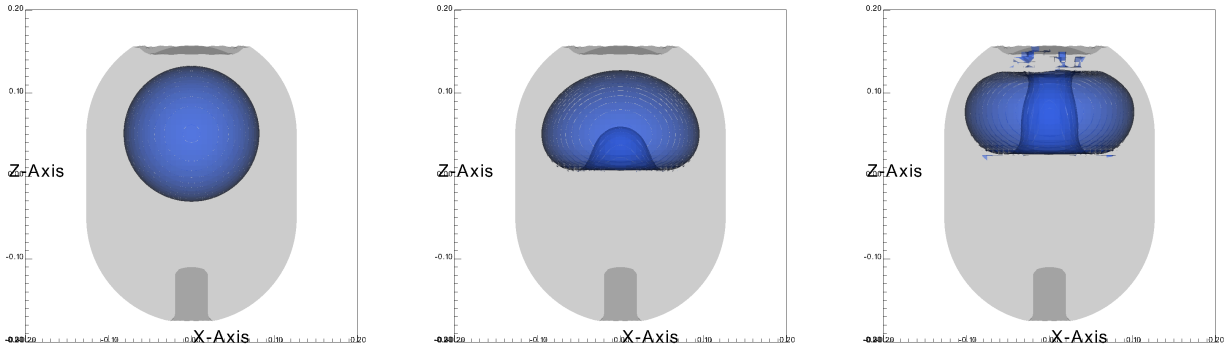

Figure: **PLSMOF**, deformation of a spherical ullage due to a liquid jet, $We_j = 5.25$. Times $t = 0.0$, 7.84, and 15.57 shown. The jet penetrates the ullage. Grid size $64 \times 64 \times 64$.

Numerical Experiments: Deformation of Spherical Ullage Due to Impinging Jet ($We_j = 5.25$)

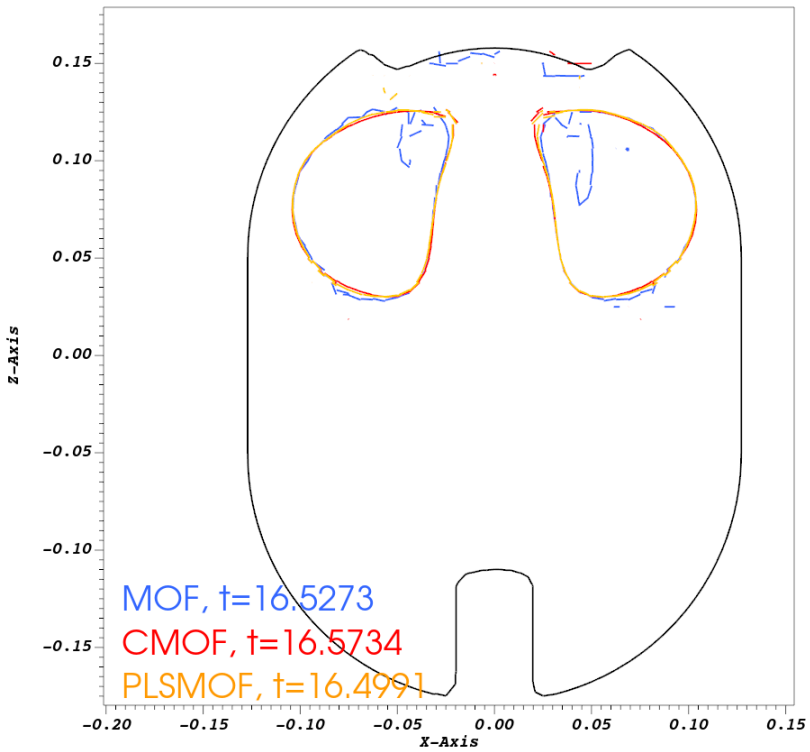

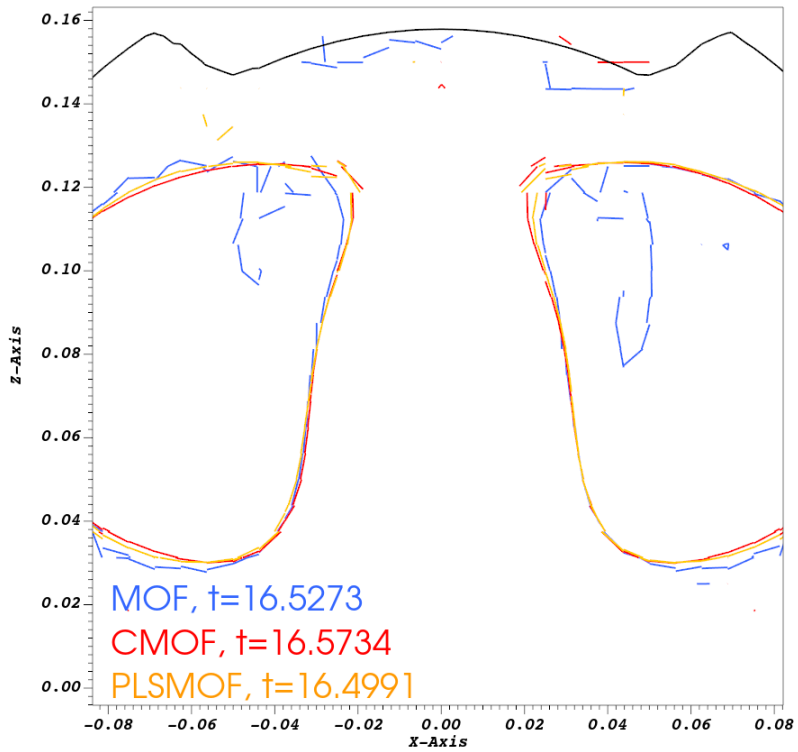

Figure: MOF, CMOF, PLSMOF comparison of vapor/liquid reconstructed interface at $t \approx 16.5$ after break-up of the spherical ullage due to an impinging jet ($We_j = 5.25$).
Grid size $64 \times 64 \times 64$.

Conclusions, takeaways

- While MOF shows better results for rigid body motion, it is a local method. Therefore it cannot 'see' surface tension effects during interface reconstruction, is subject to checkerboard instability.
- CMOF and PLSMOF use information in neighborhood during cell reconstruction, able to damp out noise.
- In low Weber/Reynolds number regimes, CMOF and PLSMOF may be more suitable than MOF
- PLSMOF speed comprable to that of MOF, while getting benefits of CMOF.
- PLSMOF generalizable to unstructured grids.
- PLSMOF is volume preserving and applicable to N-phase flow problems involving more than ≥ 2 materials.

REFERENCES

[1] M Bentz, J Meserole, and R Knoll. "Jet mixing in low gravity-Results of the Tank Pressure Control Experiment". In: *28th Joint Propulsion Conference and Exhibit*. 1992, p. 3060.

[2] M Bentz et al. "Low-g fluid mixing-Further results from the Tank Pressure Control Experiment". In: *29th Joint Propulsion Conference and Exhibit*. 1993, p. 2423.

[3] Vadim Dyadechko and Mikhail Shashkov. "Moment-of-fluid interface reconstruction". In: *Los Alamos report LA-UR-05-7571* (2005).

[4] Douglas Enright et al. "A Hybrid Particle Level Set Method for Improved Interface Capturing". In: *Journal of Computational Physics* 183.1 (2002), pp. 83 –116.

[5] Hui Hu and Zheyan Jin. "An icing physics study by using lifetime-based molecular tagging thermometry technique". In: *International Journal of Multiphase Flow* 36.8 (2010), pp. 672–681.

[6] Matthew Jemison et al. "A coupled level set-moment of fluid method for incompressible two-phase flows". In: *Journal of Scientific Computing* 54.2-3 (2013), pp. 454–491.

[7] Junseok Kim. "Phase field computations for ternary fluid flows". In: *Computer methods in applied mechanics and engineering* 196.45 (2007), pp. 4779–4788.

[8] Antoine Lemoine, Stéphane Glockner, and Jérôme Breil. "Moment-of-fluid analytic reconstruction on 2D Cartesian grids". In: *Journal of Computational Physics* 328 (2017), pp. 131–139.

[9] Guibo Li et al. “Incompressible multiphase flow and encapsulation simulations using the moment-of-fluid method”. In: *International Journal for Numerical Methods in Fluids* 79.9 (2015), pp. 456–490. eprint: https://onlinelibrary.wiley.com/doi/pdf/10.1002/fld.4062.

[10] Sean Mauch. “A fast algorithm for computing the closest point and distance transform”. In: *Go online to http://www. acm. caltech. edu/seanm/software/cpt/cpt. pdf* 2 (2000).

[11] Thomas Milcent and Antoine Lemoine. “Moment-of-fluid analytic reconstruction on 3D rectangular hexahedrons”. In: *Journal of Computational Physics* 409 (2020), p. 109346.

[12] C. Pei et al. “A Hierarchical Space-Time Spectral Element and Moment-of-Fluid Method for Improved Capturing of Vortical Structures in Incompressible Multi-phase/Multi-material Flows”. In: *J. Sci. Comput.* 81 (2019), pp. 1527–1566.

[13] Chaoxu Pei et al. “A hierarchical space-time spectral element and moment-of-fluid method for improved capturing of vortical structures in incompressible multi-phase/multi-material flows”. In: *Journal of Scientific Computing* 81.3 (2019), pp. 1527–1566.

[14] Mark Sussman. “A second order coupled level set and volume-of-fluid method for computing growth and collapse of vapor bubbles”. In: *Journal of Computational Physics* 187.1 (2003), pp. 110–136.

[15] Mehdi Vahab, Mark Sussman, and Kourosh Shoele. “Fluid-structure interaction of thin flexible bodies in multi-material multi-phase systems”. In: *Journal of Computational Physics* 429 (2021), p. 110008.

[16] Truong V Vu et al. “Numerical investigations of drop solidification on a cold plate in the presence of volume change”. In: *International Journal of Multiphase Flow* 76 (2015), pp. 73–85.

[17] Zhouteng Ye et al. “An Improved Coupled Level Set and Continuous Moment-of-Fluid Method for Simulating Multiphase Flows with Phase Change”. In: *Communications on Applied Mathematics and Computation* (Aug. 2023).